ChemComm

COMMUNICATION

View Article Online
View Journal

Check for updates

Cite this: DOI: 10.1039/d5cc00369e

Received 20th January 2025,
Accepted 18th February 2025

DOI: 10.1039/d5cc00369e

rsc.li/chemcomm

Published on 18 February 2025. Downloaded by Shanghai Normal University on 2/25/2025 12:49:36 AM.

Visual detection of HPV16 using a photoactivatable CRISPR–Cas12 system†

Xiaoya Gu,[a] Zhe Ma,[b] Lin Zhou,[a] Na Li,[a] Shijiang Yu,[b] Fu Wang *[bc] and Ruifang An*[a]

Human papillomavirus (HPV) screening is crucial for the diagnosis of cervical cancer. In this study, we have combined photoactivated CRISPR–Cas12a with tube-in-tube structure and recombinase polymerase amplification (RPA) to enable simple, rapid and convenient visualization detection of HPV16, facilitated by blue UV light at 302 nm. It serves as a potential tool for on-site diagnostic use, which could be beneficial in terms of portability and speed.

It is estimated that around 80% of women will be infected with HPV at some point in their lives. In the majority of cases, the immune system is able to clear the virus within 12 to 24 months. However, persistent high-risk HPV infections have been linked to the development of associated conditions such as cervical cancer.[1] That's why HPV testing is so important.[2] Two main categories of HPV detection methods are used to test uterine cervical specimens: signal amplification techniques (liquid phase hybridization techniques) and target amplification techniques (gene amplification or polymerase chain reaction, PCR).[3] Real-time quantitative PCR is a widely used method that offers superior sensitivity and specificity, high detection throughput, and ease of automation. However, the technique is not without limitations that limit its full potential. For example, the number of HPV genotypes that can be identified in a single PCR reaction is limited by the fluorescent channel.[4] In addition, the high cost of the necessary equipment and reagents poses a significant challenge in regions with limited medical resources.[5] More recently, the advent of the CRISPR–Cas detection system has led to significant advances in HPV detection in recent years(*e.g.*, SHERLOCK, DETECTR).[6] These developments have the potential to overcome the limitations of traditional[7] diagnostic methods, particularly in pathogen detection.[8] In addition, CRISPR technology offers significant advantages over the traditional nucleic acid assays in terms of cost, efficiency, portability, and uniqueness.

CRISPR–Cas is a recently developed biotechnology tool that shows great promise.[9] In order to increase the sensitivity of the CRISPR detection reaction, it is recommended that nucleic acid amplification be performed beforehand. However, this approach poses a significant challenge due to the incompatibility between recombinase polymerase amplification (RPA) and CRISPR. The efficiency and sensitivity of nucleic acid amplification can be affected by *cis* cleavage and the reaction buffer used in CRISPR.[10,11] As a result, most current CRISPR nucleic acid detection strategies consist of two distinct steps. It is important to note that this can indirectly lead to an increase in the number of steps required, an increased risk of contamination, and an increased likelihood of false positives. A number of potential solutions have been proposed to address this issue, including the use of superior one-pot buffers, the design and screening of suboptimal PAM sites,[12] and the spatial isolation of the components.[13] Microfluidics[14] and dynamic aqueous multiphase reaction (DAMR) systems[15] have also been incorporated. Nevertheless, these strategies remain limited due to the problem of incompatibility.

Photoactivatable CRISPR technology represents a transformative approach, offering unprecedented control with non-invasive, high spatial and temporal precision.[16] In recent years, a number of CRISPR systems using ultraviolet (UV),[17] blue[7] and red light[18,19] have been developed and applied in various fields, including gene editing, biosensing and tumour therapy.[20–23] Current methods for photoactivation of CRISPR involve the use of photoactivatable nanocarriers for Cas proteins,[24] guide RNAs and RNP complexes. In the context of light-activated CRISPR biosensing, the use of transiently silenced crRNA, achieved by incorporating the photocleavable motif 6-nitro-piperidoxymethyl (NPOM) into the crRNA,[25] or a complementary single-stranded RNA (p-RNA) containing photocleavable (PC) linkers, has led to

[a] Department of Obstetrics and Gynecology, The First Affiliated Hospital of Xi'an Jiaotong University, Xi'an Jiaotong University, Xi'an 710061, China. E-mail: anruifang@xjtu.edu.cn
[b] Institute of Medical Engineering, School of Basic Medical Sciences, Xi'an Jiaotong University, Xi'an 710061, China. E-mail: wangfu@xjtu.edu.cn
[c] Department of Urology, The Second Affiliated Hospital of Xi'an Jiaotong University, Xi'an, Shaanxi 710004, China

† Electronic supplementary information (ESI) available. See DOI: https://doi.org/10.1039/d5cc00369e

Published on 18 February 2025. Downloaded by Shanghai Normal University on 2/25/2025 12:49:36 AM.

remarkable sensitivity and specificity in nucleic acid assays. For non-nucleic acid detection, signal transduction and amplification techniques are often used. For example, a light-activated one-pot RCA-Cas12a method has been developed for simple and highly sensitive detection of *S. aureus* using aptamers and silencing of crRNA with photocleavable ssDNA (PC-DNA).[26] In addition to these applications, light-based CRISPR systems have also been used for intracellular imaging.[27]

In this study, we have developed a photoactivatable CRISPR–Cas12a system for rapid and cost-effective detection of HPV 16 in a single step. The crRNA in our system is decorated with three 6-nitropiperonyloxymethyl-caged thymidine (NPOM-dt)[25,28,29] molecules and is lengthened at the 3′-end with seven DNA-extended (TATTATT) sequences, collectively abbreviated as 3N-crRNA. In our scenarios, the Watson–Crick base pairing between 3N-crRNA and target DNA was disrupted by a steric hindrance effect. This can be reversed by the process of decaging, which is facilitated by UV light. To enhance the fluorescence for visual inspection, the CRISPR–Cas12a system was integrated into a tube-in-tube structure, which consists of an outer PCR tube and an inner tube containing two hydrophobic holes. We demonstrated that the RPA-assisted photoactivatable CRISPR–Cas12a with a tube-in-tube structure enables efficient visual HPV diagnostics that circumvents the open cap step. It is anticipated to be a valuable point-of-care testing (POCT) tool for rapid, self-testing of HPV in applications with limited healthcare resources.

As shown in Fig. 1A and B, in addition to the 6-nitropiperoyloxymethyl cage thymidine (NPOM-dt) incorporated into the crRNA (designed for the HPV16-L1 gene) of the Lachnospiraceae bacterium ND2006 Cas12a (LbCas12a), a 7-base DNA extension (TATTATT) was also performed at its 3′ end, termed photoactivatable crRNA (3N-crRNA). To explore the efficacy of the photoactivatable CRISPR/Cas12a, we investigated the cleavage of ssDNA indicator (ssDNA of 30 nt) and generation of fluorescent signal from the ssDNA-FQ reporter. As supported by the results of the microplate reader (Fig. 1C and D) and the native polyacrylamide gel electrophoresis (PAGE) (Fig. 1E), after 30 s UV irradiation at 365 nm and incubation at 37 °C for 20 min in the dark, the NPOM modified in the nitrogen heterocycle of thymidine could be rapidly discharged, and the trans-cleavage activity of CRISPR–Cas12a mediated by photoactivated crRNA (3N-crRNA) was significantly higher than that of ordinary crRNA (2.4-fold), although its fluorescence intensity was slightly reduced compared to that of the engineered crRNA with 7-base DNA extension at 3′ end (3-crRNA). Further investigation revealed that this photoactivatable crRNA showed sufficient stability without any leakage when exposed to ambient light after 8 h at room temperature, although its activity was slightly reduced compared with that in avoid light (Fig. S1A and S2A, ESI†). The further study showed that the detection performance was the best when the light intensity was 35 W (Fig. S1B and C, ESI†) and at the height from the tube was 5 cm (Fig. S1D and S2B, ESI†). We then evaluated the light duration time of 3N-crRNA and found that the optimal signal-to-noise ratio could be achieved when 365 nm light was applied for 30 s (Fig. S1E and F, ESI†). Furthermore, the detection performance was the best when the concentration of LbCas12a was 20 nM (Fig. S1G and H, ESI†) and the ratio of LbCas12a to 3N-crRNA was 1 : 1 (Fig. S1I and S2C, ESI†).

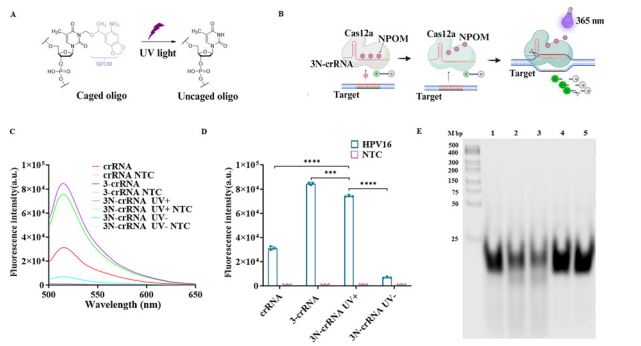


Fig. 1 Design and validation of photoactivatable CRISPR–Cas12a system. (A) Structure of NPOM-modified caged thymidine. Thymidine degradation is achieved by irradiation with UV light. (B) Schematic of photoactivatable CRISPR/Cas12a for nucleic acid detection. (C) Comparison of the fluorescence intensity of the CRISPR–Cas12a reaction using ordinary crRNA, engineered crRNA with 7-base DNA extension at 3′ end (3-crRNA), photoactivatable crRNA (3N-crRNA) with HPV16 or NTC. (D) Quantification of the fluorescence intensity in (C). (E) Native PAGE analysis of trans-cleavage activity of LbCas12a with different crRNA: (1) crRNA; (2) 3-crRNA; (3) 3N-crRNA UV +; (4) 3N-crRNA UV-; (5) ssDNA indicator (30 nt). (NTC: No target control, ***$P < 0.001$, ****$P < 0.0001$).

Following by the exploration of the photoactivatable CRISPR/Cas12a assay, we evaluated the efficiency of the assay when combined with the recombinase polymerase amplification (RPA) reaction. Initially, we optimized the concentration of primer, MgOAc, and ssDNA-FQ probe in the conventional photoactivatable CRISPR/Cas12a combined with RPA assay. Based on the results, the efficiency was optimal when the primer concentration was 0.3 μM (Fig. S3A, ESI†) and the MgOAc concentration was 14 mM (Fig. S3B, ESI†). With the increasing concentration of the ssDNA-FQ probe, the fluorescence signal intensity improved accordingly (Fig. S3C, ESI†). The final fluorescence also showed that the limit detection performance of conventional photoactivatable CRISPR–Cas12a assisted by RPA was still better than that of normal crRNA on a variety of HPV16 plasmids at different concentrations (Fig. S3D–F and S4A–C, ESI†). Meanwhile, the detection efficiency with 3N-crRNA was comparable to that with 3-crRNA.

Considering that the original intention of the optical control was to solve the incompatibility problem, we next evaluated the performance of photoactivated CRISPR/Cas12 with RPA in one-pot assay (Fig. 2A). First, we investigated the optimal concentration of primer, MgOAc, and ssDNA-FQ probe in one-pot assay. As shown in Fig. 2B and C, the primer at 0.4 μM (Fig. 2B) and the MgOAc at 16 mM (Fig. 2C) could achieve the best performance in the one-pot assay. For the ssDNA-FQ probe, the fluorescence intensity increased according to the increasing concentration of ssDNA (Fig. 2D). In the light-controlled one-pot assay, the presence of the primers would increase the background signal of fluorescence. We then designed and examined the 8 pairs of primers for the HPV-16-L1 gene in the RPA reaction (Fig. 2E). The results showed that the presence of the primers increased the fluorescence of the no target control (NTC) in the one-pot

 This journal is © The Royal Society of Chemistry 2025

Published on 18 February 2025. Downloaded by Shanghai Normal University on 2/25/2025 12:49:36 AM.

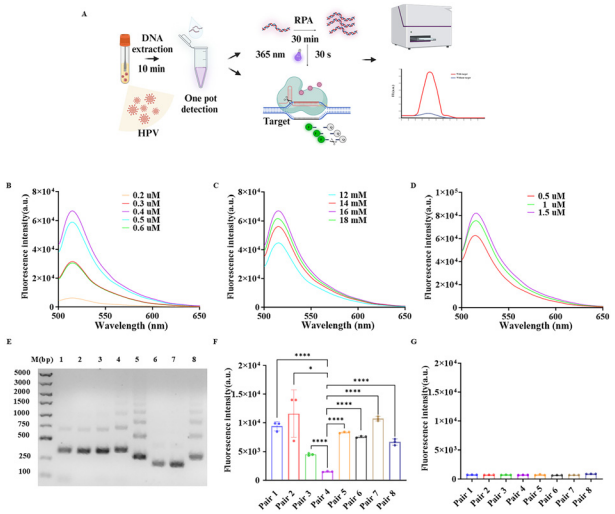


Fig. 2 One-pot photoactivatable CRISPR/Cas12a combined with RPA assay. (A) Schematic of one-pot photoactivatable CRISPR/Cas12a combined with RPA assays. (B) Optimization of primer concentration. (C) Optimization of MgOAc concentration. (D) Optimization of ssDNA-FQ probe concentration. (E) Results of 1% agarose gel electrophoresis analysis of RPA products for 8 primer pairs. (F) Background signals of 8 of primer pairs in the one-pot photoactivatable CRISPR/Cas12a combined with RPA assays. (G) Background signals of 8 primer pairs in the only photoactivatable CRISPR/Cas12a reaction. (NTC: No target control, $*P < 0.05$, $****P < 0.0001$).

photoactivatable CRISPR–Cas12a with RPA assay (Fig. 2F), which didn't occur in the only photoactivatable CRISPR–Cas12a reaction (Fig. 2G). Therefore, primer pair 4 was thus selected for the subsequent reaction to reduce the false positive rate. As hypothesized, the one-pot photoactivated CRISPR–Cas12a with RPA was able to discriminate HPV16 plasmid at concentrations of 10^{-18} M from NTC (Fig. S5A and B, ESI†), which can't be achieved by the one-pot assay with crRNA (Fig. S5C, ESI†) nor 3-crRNA (Fig. S5D, ESI†).

Despite the excellent performance of the one-pot photoactivated CRISPR/Cas12a with RPA assay, its fluorescence intensity is still not sufficient for visual detection. To facilitate the result output, we introduced a tube-in-tube structure in an attempt to increase the fluorescence intensity for visual detection (Fig. 3A). The inner tube was designed for the RPA reaction, containing two hydrophobic pores on both sides. As illustrated in Fig. 3B, simply by performing the RPA reaction (37 °C for 30 min in the inner tube), a brief centrifugation (600 rpm) for 1 min or vigorous shaking could mix the products of RPA with the photoactivatable CRISPR–Cas12a components stored in the outer tube through the hydrophobic pores.[30] The photoactivatable CRISPR–Cas12a reaction was then initiated after 30 seconds of UV light at 365 nm. The tube-in-tube structure was finally photographed under 302 nm to record the results after incubation at 37 °C for 20 min. To check whether the tube-in-tube structure could successfully transfer RPA components from the inner tube to the outer tube through the hydrophobic pores, trypan blue solution was added to 15 μl of RPA reaction buffer. As shown in Fig. 3C and D, almost no liquid leaked from

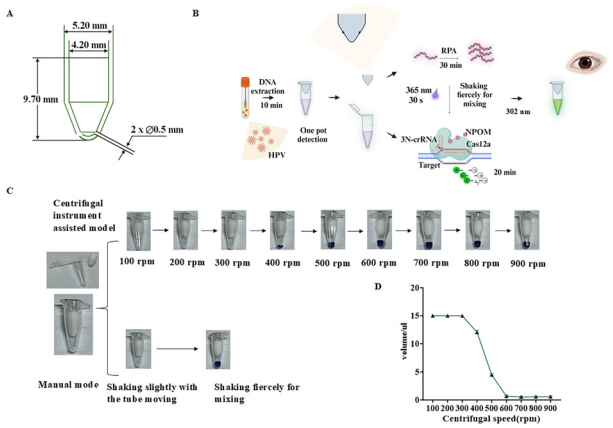


Fig. 3 Design of a tube-in-tube structure for HPV detection. (A) Schematic diagram of the inner tube structure. (B) Detection procedure for one-pot photoactivatable CRISPR/Cas12a with tube-in-tube structure. (C) Schematic diagram of the tube-in-tube structure transferring inner casing solution condition requirements. (D) The volume of liquid remaining in the inner tube at different centrifuge speeds.

the inner tube when the tube was gently shaken, capped and moved, whereas all the RPA reaction buffer in the inner tube could be completely transferred to the outer tube by vigorous shaking or centrifugation (600 rpm).

As the gap and distance between the inner and outer tubes may affect the optimum reaction temperature, we carried out a series of tests. Based on our results, the final fluorescence at 37 °C and 39 °C could be distinguished by the naked eye under 302 nm (Fig. 4A and Fig. S6A, B, ESI†). However, the final fluorescence observed by the naked eye was significantly reduced at 45 °C and couldn't be seen by the naked eye at 48 °C. For

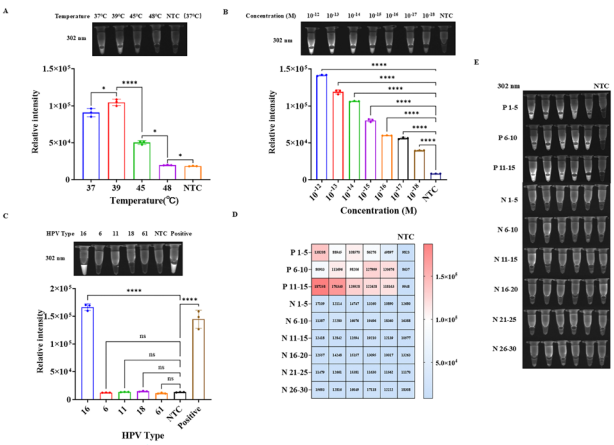


Fig. 4 HPV16 visual detection by photoactivatable CRISPR–Cas12 with tube-in-tube structure. (A) The effect of different temperatures on the final visual signal. (B) Sensitivity of photoactivatable CRISPR–Cas12 system with tube-in-tube structure. (C) Specificity of photoactivatable CRISPR–Cas12 with tube-in-tube structure. (D) and (E) Photoactivatable CRISPR–Cas12 system with tube-in-tube structure was further applied to the detect of HPV16 in real clinical samples. (NTC: no target control, positive: HPV16-L1 plasmids, N: negative clinical samples validated by qPCR, P: positive clinical samples validated by qPCR, $^{ns}P > 0.05$, $*P < 0.05$, $***P < 0.001$, $****P < 0.0001$).

Published on 18 February 2025. Downloaded by Shanghai Normal University on 2/25/2025 12:49:36 AM.

reasons of portability, 37 °C, the temperature of the human body was used as the optimum to ensure the efficiency of our system under modest conditions. Subsequently, we tested the sensitivity and selectivity of the photoactivated CRISPR–Cas12a with tube-in-tube structure under the above optimal conditions. As shown in Fig. 4B and Fig. S6D, E (ESI†), for the sensitivity test, our system can discriminate HPV plasmids with concentrations of 10^{-18} M from NTC by the naked eye under 302 nm. For the specificity test, clinical samples of HPV16, HPV6, HPV11, HPV18, and HPV61 were selected, and the reaction produced visually distinguishable signals only when HPV16 samples were added (Fig. 4C and Fig. S6C, S7A, ESI†). To evaluate the feasibility of our system for HPV testing, 15 HPV16-positive samples and 30 HPV16-negative samples identified by quantitative PCR (qPCR) (Fig. S7B and C, ESI†) were collected. As expected, the HPV16 detection accuracy reached 93.33%, which is consistent with the clinical records (Table S2, ESI†). Among the samples, only 1 positive sample (#5) was misdiagnosed as negative (Fig. 4D, E and Fig. S6F, ESI†).

In this study, we have developed a photoactivated CRISPR–Cas12a system with a tube-in-tube structure for the visualization detection of HPV16. In particular, in comparison with the current two-step RPA-Cas12a detection method, this system is more straightforward and circumvents the steps of opening the lid and transferring the liquid, which reduces the probability of aerosol contamination. Furthermore, the suitable temperature and simplicity of operation make it suitable for use in areas with limited medical resources. We believe that our photoactivated CRISPR–Cas12a system with tube-in-tube structure may provide an opportunity for on-site diagnostic use.

This study has been approved by The Biomedical Ethics Committee of Health Science Center of Xian Jiaotong University (Approval No. XJTU1AF2023LSK-502). Clinical cervical swab samples were obtained from the The First Affiliated Hospital of Xi'an Jiaotong University were used for the assay. The informed consent was obtained from human subjects.

We acknowledge financial support from the National Natural Science Foundation of China (No. 32271512), Natural Science Basic Research Program of Shaanxi (No. 2022JC-56, 2023-JC-ZD-43), The Foreign Expert Project of Ministry of Science and Technology of China (No. G2023174001L).

Data availability

The data supporting this article have been included as part of the ESI.†

Conflicts of interest

The authors declare that they have no competing interests.

Notes and references

1 R. J. Huang, Z. M. Liu, T. S. Sun and L. Zhu, *Microbiol. Res.*, 2024, **287**, 127857.
2 O. Reich and S. Regauer, *Virus Res.*, 2023, **329**, 199068.
3 H. Debaque and M. L. Eide, *Ann. Pathol.*, 2012, **32**, 401–409.
4 S. Naegele, D. A. Ruiz-Torres, Y. Zhao, D. Goss and D. L. Faden, *J. Mol. Diagn.*, 2024, **26**, 179–190.
5 A. Letafati, A. V. Farahani, M. M. B. Nasiri, H. Pourmoein, O. S. Ardekani, H. Ahoodashty, M. B. Hashemi-Soteh, A. Dadgar, P. Behshood, I. R. Azhar and M. Parsania, *Virol. J.*, 2024, **21**, 227.
6 M. Bartosik, L. Moranova, N. Izadi, J. Strmiskova, R. Sebuyoya, J. Holcakova and R. Hrstka, *J. Med. Virol*, 2024, **96**, e29409.
7 W. F. Zhang, H. Z. Wang, Z. T. Luo, Y. Z. Jian, C. Y. Gong, H. Wang, X. J. Lin, M. L. Liu, Y. M. Wang and H. W. Shao, *Mol. Ther.*, 2024, **32**, 920–934.
8 Z. Razavi, M. Soltani, M. Souri and H. Pazoki-Toroudi, *Crit. Rev. Anal. Chem.*, 2024, 1–25.
9 T. Huang, R. Zhang and J. M. Li, *J. Adv. Res.*, 2023, **50**, 69–82.
10 J. E. van Dongen, J. T. W. Berendsen, R. D. M. Steenbergen, R. M. F. Wolthuis, J. C. T. Eijkel and L. I. Segerink, *Biosens. Bioelectron.*, 2020, **166**, 112445.
11 J. Zhou, Z. Li, J. S. Olajide and G. Wang, *Heliyon*, 2024, **10**, e26179.
12 S. H. Lu, X. H. Tong, Y. Han, K. Zhang, Y. Z. Zhang, Q. B. Chen, J. Y. Duan, X. L. Lei, M. H. Huang, Y. Qiu, D. Y. Zhang, X. Zhou, Y. Zhang and H. Yin, *Nat. Biomed. Eng.*, 2022, **6**, 286.
13 Y. Q. Wang, Y. Q. Ke, W. J. Liu, Y. Q. Sun and X. T. Ding, *ACS Sens.*, 2020, **5**, 1427–1435.
14 Z. C. Xu, D. J. Chen, T. Li, J. Y. Yan, J. Zhu, T. He, R. Hu, Y. Li, Y. H. Yang and M. L. Liu, *Nat. Commun.*, 2022, **13**, 6480.
15 K. Yin, X. Ding, Z. Y. Li, H. Zhao, K. Cooper and C. C. Liu, *Anal. Chem.*, 2020, **92**, 8561–8568.
16 S. Y. Wang, J. Q. Wang, B. J. Li and J. J. Zhang, *ChemBioChem*, 2024, **25**, e202400685.
17 E. V. Moroz-Omori, D. Satyapertiwi, M. C. Ramel, H. Hogset, I. K. Sunyovszki, Z. Q. Liu, J. P. Wojciechowski, Y. Y. Zhang, C. L. Grigsby, L. Brito, L. Bugeon, M. J. Dallman and M. M. Stevens, *Acs Central Sci.*, 2020, **6**, 695–703.
18 X. H. Chen, Y. X. Chen, H. H. Xin, T. Wan and Y. Ping, *Proc. Natl. Acad. Sci. U. S. A.*, 2020, **117**, 2395–2405.
19 J. W. Shao, M. Y. Wang, G. L. Yu, S. H. Zhu, Y. Yu, B. C. Heng, J. L. Wu and H. F. Ye, *Proc. Natl. Acad. Sci. U. S. A.*, 2018, **115**, E6722–E6730.
20 R. S. Zou, Y. Liu, B. Wu and T. Ha, *Mol. Cell*, 2021, **81**, 1553.
21 O. Semikolenova, L. Sakovina, E. Akhmetova, D. Kim, I. Vokhtantsev, V. Golyshev, M. Vorobyeva, S. Novopashin and D. Novopashina, *Int. J. Mol. Sci.*, 2021, **22**, 10919.
22 T. Hu, Y. Y. Yu, Y. Lin and C. X. Chen, *Anal. Chem.*, 2023, **95**, 18587–18594.
23 H. L. Tang, X. J. Xu, Y. X. Chen, H. H. Xin, T. Wan, B. W. Li, H. M. Pan, D. Li and Y. Ping, *Adv. Mater.*, 2021, **33**, e2006003.
24 E. Cho, D. Yun and C. Jung, *Sens. Actuators, B*, 2024, **412**, 135790.
25 M. L. Hu, R. H. Liu, Z. Q. Qiu, F. Cao, T. Tian, Y. X. Lu, Y. Z. Jiang and X. M. Zhou, *Angew. Chem., Int. Ed.*, 2023, **62**, e202300663.
26 Q. Wu, S. Jiang, Y. Huang, L. J. Zhang, Z. Y. Li, Y. B. Hou, J. Zhang, Y. W. Wang, C. L. Zhu, D. D. Zhou, W. X. Chen and D. D. Li, *Chem. Eng. J.*, 2023, **477**, 146814.
27 H. Liu, J. T. Dong, Z. J. Duan, F. Xia, I. Willner and F. J. Huang, *Sci. Adv.*, 2024, **10**, eadp6166.
28 A. Deiters, R. A. Garner, H. Lusic, J. M. Govan, M. Dush, N. M. Nascone-Yoder and J. A. Yoder, *J. Am. Chem. Soc.*, 2010, **132**, 15644–15650.
29 W. Y. Zhou, W. Brown, A. Bardhan, M. Delaney, A. S. Ilk, R. R. Rauen, S. I. Kahn, M. Tsang and A. Deiters, *Angew. Chem., Int. Ed.*, 2020, **59**, 8998–9003.
30 F. Hu, Y. F. Liu, S. H. Zhao, Z. M. Zhang, X. C. Li, N. C. Peng and Z. D. Jiang, *Biosens. Bioelectron.*, 2022, **202**, 113994.

 This journal is © The Royal Society of Chemistry 2025